nature physics

LETTERS

https://doi.org/10.1038/s41567-017-0020-9

Signatures of a dissipative phase transition in photon correlation measurements

Thomas Fink[1*], Anne Schade[2], Sven Höfling[2,3], Christian Schneider[2] and Ataç Imamoglu[1]

Understanding and characterizing phase transitions in driven-dissipative systems constitutes a new frontier for many-body physics[1–8]. A generic feature of dissipative phase transitions is a vanishing gap in the Liouvillian spectrum[9], which leads to long-lived deviations from the steady state as the system is driven towards the transition. Here, we show that photon correlation measurements can be used to characterize the corresponding critical slowing down of non-equilibrium dynamics. We focus on the extensively studied phenomenon of optical bistability in GaAs cavity polaritons[10,11], which can be described as a first-order dissipative phase transition[12–14]. Increasing the excitation strength towards the bistable range results in an increasing photon-bunching signal along with a decay time that is prolonged by more than nine orders of magnitude as compared with that of single polaritons. In the limit of strong polariton interactions leading to pronounced quantum fluctuations, the mean-field bistability threshold is washed out. Nevertheless, the functional form with which the Liouvillian gap closes as the thermodynamic limit is approached provides a signature of the emerging dissipative phase transition. Our results establish photon correlation measurements as an invaluable tool for studying dynamical properties of dissipative phase transitions without requiring phase-sensitive interferometric measurements.

Bistability, the coexistence of two stable states with different photon number under the same driving conditions, is a general signature of driven-dissipative nonlinear systems, and is commonly observed in a broad range of experimental realizations[10,11,15–17]. This phenomenon can be well understood by treating the system in a mean-field description, that is, replacing the system's creation and annihilation operators by their corresponding expectation values. Neglecting quantum fluctuations in this way leads to diverging lifetimes of the two (otherwise metastable) states and results in hysteretic behaviour when the excitation power is ramped. A full quantum treatment, on the other hand, predicts a unique steady state with no indication of the underlying bistability[12,18]. These two pictures can be reconciled by investigating quantum non-equilibrium dynamics, described by a Liouvillian superoperator. In analogy with the spectrum of a Hamiltonian, the real part of the Liouvillian eigenvalues corresponds to the decay rate of the respective eigenmodes. The steady state of the driven-dissipative evolution is the eigenmode of the Liouvillian with zero eigenvalue. In the bistable regime, the Liouvillian excitation gap, or the asymptotic decay rate of its first excited state, vanishes in the thermodynamic limit (where the number of system excitations/particles $N \to \infty$), corresponding to a diverging lifetime of a second eigenmode. The latter can exceed all intrinsic timescales by many orders of magnitude and is the reason for the successful description of bistability experiments by mean-field theory[19]. In general, a vanishing Liouvillian excitation gap signals a dissipative phase transition (DPT)[9,13,14,20,21].

Here, we demonstrate that the asymptotic decay rate of the Liouvillian can be determined by measuring photon correlations in a Hanbury Brown and Twiss (HBT) set-up. Due to the coexistence of a high- and low-intensity state, detection of a first photon corresponds to a weak measurement of a high-photon-number state, which in turn results in a higher probability to simultaneously detect a second photon compared with the average photon detection rate. This leads to a photon-bunching signal, where the magnitude of bunching depends on the system nonlinearity and laser detuning. More importantly, the timescale over which the bunching persists depends on the decay rate towards the steady state, and therefore reveals information about the Liouvillian gap (Supplementary Information). We emphasize that the corresponding photon bunching may well exceed two, indicating that photon correlations can be much stronger than those in thermal states of light. The recently introduced technique of dynamical hysteresis in principle also allows to extract the Liouvillian gap[22]. However, the requirement to sweep the excitation power non-adiabatically restricts these measurements to regimes close to the thermodynamic limit with vanishing gap and diverging timescales, making the technique unsuitable for the cases considered here.

Figure 1a shows the schematic of the experiment where a fibre cavity incorporating an InGaAs quantum well (QW) is driven by a single-mode laser field (see Methods). Application of a d.c. voltage to a nanopositioner that controls the distance between fibre and sample allows for the in situ tuning of the cavity energy with respect to the QW exciton resonance. Sweeping this voltage while recording the transmission spectrum under broadband illumination (Fig. 1b) results in an anticrossing, demonstrating the strong coupling between cavity photons and QW excitons. The new eigenstates of the coupled system are the lower and upper polaritons. The large splitting between the fundamental longitudinal transverse electromagnetic (TEM_{00}) and next $TEM_{10,01}$ modes of 11.8 meV illustrates the strong transverse confinement generated by the curvature of the fibre distributed Bragg reflector (DBR). Driving the TEM_{00} mode of the lower polariton branch near resonantly constitutes a realization of a driven-dissipative system with Kerr-type nonlinear interactions. The corresponding Hamiltonian in a polariton basis rotating with the excitation laser frequency is

$$\hat{H} = \Delta \hat{a}^\dagger \hat{a} + \frac{U}{2} \hat{a}^\dagger \hat{a}^\dagger \hat{a} \hat{a} + F^* \hat{a}^\dagger + F \hat{a} \qquad (1)$$

where $\hat{a}$ is a polariton annihilation operator, $\Delta = E_L - E_P$ is the detuning between excitation laser and polariton mode energy, U is the single-particle polariton–polariton interaction and F is the laser

[1]Institute of Quantum Electronics, ETH Zürich, Zürich, Switzerland. [2]Technische Physik, Universität Würzbug, Würzburg, Germany. [3]SUPA, School of Physics and Astronomy, University of St Andrews, St Andrews, UK. *e-mail: finkt@phys.ethz.ch

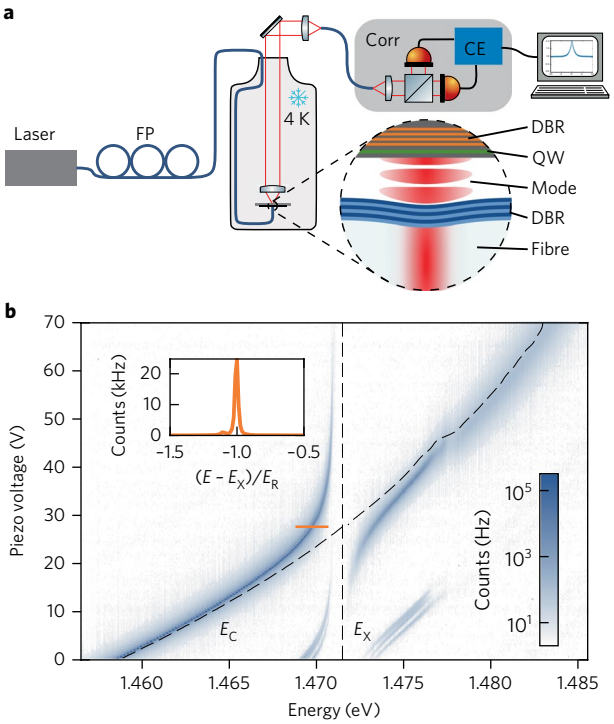

Fig. 1 | Experimental set-up and cavity transmission spectrum. **a**, Intensity-stabilized continuous-wave laser light is coupled into the cavity via optical fibres (blue lines). Fibre paddles (FP) are used to control the polarization. The transmitted signal is directed onto the correlation set-up (Corr). Two APDs in a HBT configuration record photon coincidences that are analysed by correlation electronics (CE). The zoom-in displays the cavity structure. **b**, Transmission spectrum under weak broadband illumination while sweeping the piezo voltage/cavity length. A clear anticrossing between the fundamental Gaussian cavity mode and exciton resonance (grey dashed lines denoted $E_{C,X}$) indicates the appearance of upper and lower polariton modes with a normal mode splitting of 3.50 meV. The multiple resonances at low piezo voltages correspond to the $TEM_{01,10}$ transverse mode manifold. At 1.478 eV, another anticrossing with smaller splitting appears that may stem from strong coupling of the cavity mode to an impurity resonance in the semiconductor. Inset: line cut along the orange line showing the lower polariton resonance. A small linear polarization splitting of 180 μeV is visible.

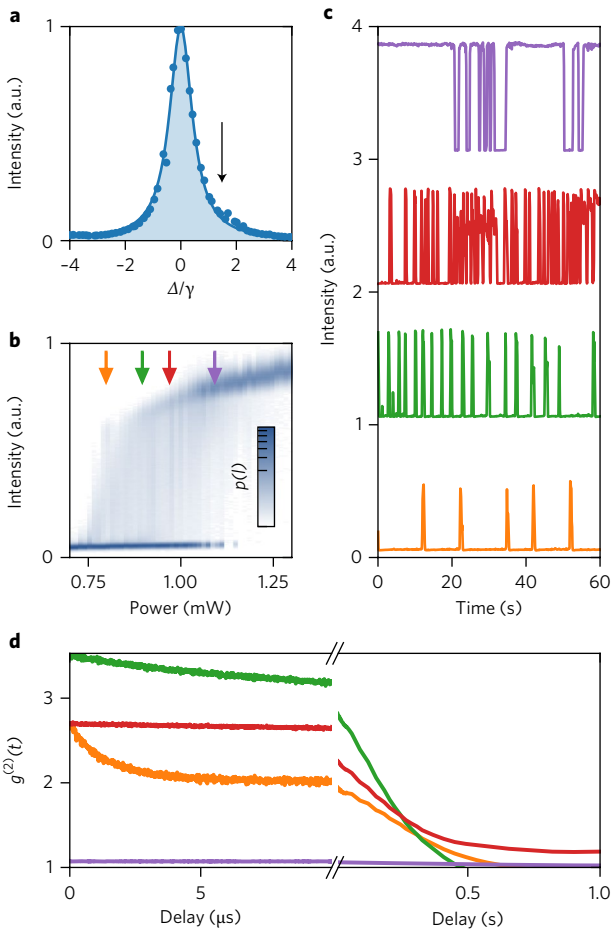

Fig. 2 | Dynamical bistability in cavity transmission. **a**, Normalized polariton transmission spectrum under weak excitation (100 nW) as a function of the laser detuning. The blue solid line is a Lorentzian fit to the data (blue circles) with a mode linewidth (FWHM) of $\gamma = 37$ μeV. The black arrow denotes the detuning of the excitation laser with respect to the polariton mode $\Delta/\gamma = 1.5$ used in **b**–**d**. **b**, Colour-coded photon number distribution $p(I)$ obtained from 150-s-long photon traces with 1 ms time binning. Between 750 and 1,200 μW, the distribution is double-peaked, indicating the bistable regime. Note the nonlinear colour scaling used to highlight the small intensity noise that occurs due to switching events faster than the binning time. The arrows denote the powers where the data in **c** and **d** were taken. **c**, Time-binned (100 ms) single photon count events normalized to the maximum intensity of all traces showing fluctuation-induced switching between the high- and low-intensity state. **d**, $g^{(2)}$ function obtained from the data in **c**. Clear photon bunching persisting up to the second scale is observed. For delays longer than 1 ms, classical intensity autocorrelations (see Methods) are shown. Note the discontinuous time axis showing both short (0–10 μs) and long (up to 1 s) dynamics.

drive strength. The nonlinearity originates from exciton–exciton interactions weighted by the exciton content of the polariton and enhanced by the strong transverse confinement. By changing the cavity–exciton detuning, we can change the lower polariton mode from a purely photonic linear cavity mode to an excitonic one with sizeable nonlinear interactions. Since polaritons decay at a rate γ, determined primarily by cavity mirror losses, the polariton dynamics obey the master equation

$$\frac{\partial\hat{\rho}}{\partial t} = \hat{\mathcal{L}}\hat{\rho}, \tag{2}$$

where

$$\hat{\mathcal{L}}\hat{\rho} = \frac{1}{i\hbar}[\hat{H},\hat{\rho}] + \frac{\gamma}{2}(2\hat{a}\rho\hat{a}^{\dagger} - \hat{a}^{\dagger}\hat{a}\rho - \rho\hat{a}^{\dagger}\hat{a}) \tag{3}$$

is the Liouvillian superoperator with γ denoting the polariton decay rate. Nonlinear driven-dissipative polariton systems described by equation (2) not only constitute a platform to test fundamental quantum optics phenomena[23,24], but are also potential candidates for applications in quantum simulations of non-equilibrium dynamics[25–29]. To investigate the dynamical signatures of dispersive bistability, we excite the polariton mode with a continuous-wave laser at a detuning of $\Delta/\gamma = 1.5$ (Fig. 2a). In this regime (that is, for $\Delta/\gamma \geq \sqrt{3}/2$), a classical description of the system has two solutions and mean-field theory predicts bistability[10,12]. Indeed, when varying the power (Fig. 2b), we observe a region where the intensity probability distribution, obtained by recording photon traces for 150 s and calculating the statistical distribution of photon counts in 1-ms-wide time bins, is peaked around two values with small and

large intensity, respectively. Recording individual photon detections then reveals the system dynamics as illustrated in Fig. 2c: we observe random switching events between a low- and high-intensity state triggered by fluctuations in the system. The timescale of these events on the order of hundreds of milliseconds corresponds to a critical slowing down by more than nine orders of magnitude compared with the bare cavity lifetime, which we measured to be 35 ps in a pulsed excitation experiment independently. This dramatic slowing down is a striking and direct signature of a DPT.

The second-order correlation function

$$g^{(2)}(t)=\frac{\langle \hat{a}^{\dagger}(t')\hat{a}^{\dagger}(t'+t)\hat{a}(t'+t)\hat{a}(t')\rangle}{\langle \hat{a}^{\dagger}(t')\hat{a}(t')\rangle^{2}} \quad (4)$$

allows for determining the dynamical properties of the polariton mode. In a nutshell, $g^{(2)}(t)$ yields the dynamics of the polariton system conditioned upon detection of a photon at time t'. The collapse operator $\hat{a}$, that is, detection of a photon, projects the system out of its steady state into a density operator $\hat{\rho}_p$ that can be written as a superposition of several Liouvillian eigenstates including the steady state. In general, we expect this state to have a finite overlap with the lowest energy Liouvillian eigenstate. The conditional dynamics following the initial photon detection are interrupted by the second photon detection event at time $t'+t$, which effectively determines polariton relaxation dynamics towards the steady state[30]. In this sense, $g^{(2)}(t)$ measures the dissipative counterpart of Hamiltonian quench dynamics. The formal requirement for obtaining super-Poissonian statistics and hence the application of our technique is that $\hat{\rho}_{ss}$ and $\hat{\rho}_p$ differ in the expectation value of the measured observable, that is, $\mathrm{Tr}\{\hat{a}^{\dagger}\hat{a}\hat{\rho}_p\} > \mathrm{Tr}\{\hat{a}^{\dagger}\hat{a}\hat{\rho}_{ss}\}$. We emphasize that this is typically the case at and around phase transitions with generically enhanced fluctuations, which makes the approach applicable to a wide range of systems.

Figure 2d shows photon correlation measurements obtained for the pump intensities indicated in Fig. 2b, where we observe a biexponential decay with two distinct timescales. The decay on the microsecond timescale strongly depends on the pump strength and we tentatively attribute this decay rate to the real part of the second excited Liouvillian eigenstate, which can also undergo a reduction as a function of drive strength (see Supplementary Information). In stark contrast, the decay of correlations in the millisecond range exhibits a much weaker dependence on the pump power. This suggests that the physics at these timescales is no longer determined only by the Liouvillian of equation (3) but rather that the influence of external classical noise sources, such as dephasing due to acoustic noise affecting the fibre cavity on these timescales, needs to be taken into account.

Whereas for detunings exceeding $\sqrt{3}/2\gamma$ mean-field theory successfully predicts the bimodal intensity distribution observed in Fig. 2b, only a single solution is obtained for smaller values and one thus expects simple dynamics. To explore if non-equilibrium dynamics exhibit a sharp detuning dependence in the presence of quantum fluctuations, we increase the polariton nonlinearity by increasing the exciton content of the lower polariton branch and change the laser detuning at which we excite the polariton mode (Fig. 3a). In Fig. 3b, we show that bunching is strongest for excitation powers at the nonlinear threshold where a power ramp exhibits a superlinear behaviour and strong photon number fluctuations occur. Above and below this region, photon statistics converge to the coherent state value $g^{(2)}(0)=1$ (Fig. 3c).

Remarkably, we observe that changing the laser detuning from the stable $(\Delta/\gamma<\sqrt{3}/2)$ to the bistable $(\Delta/\gamma>\sqrt{3}/2)$ regime

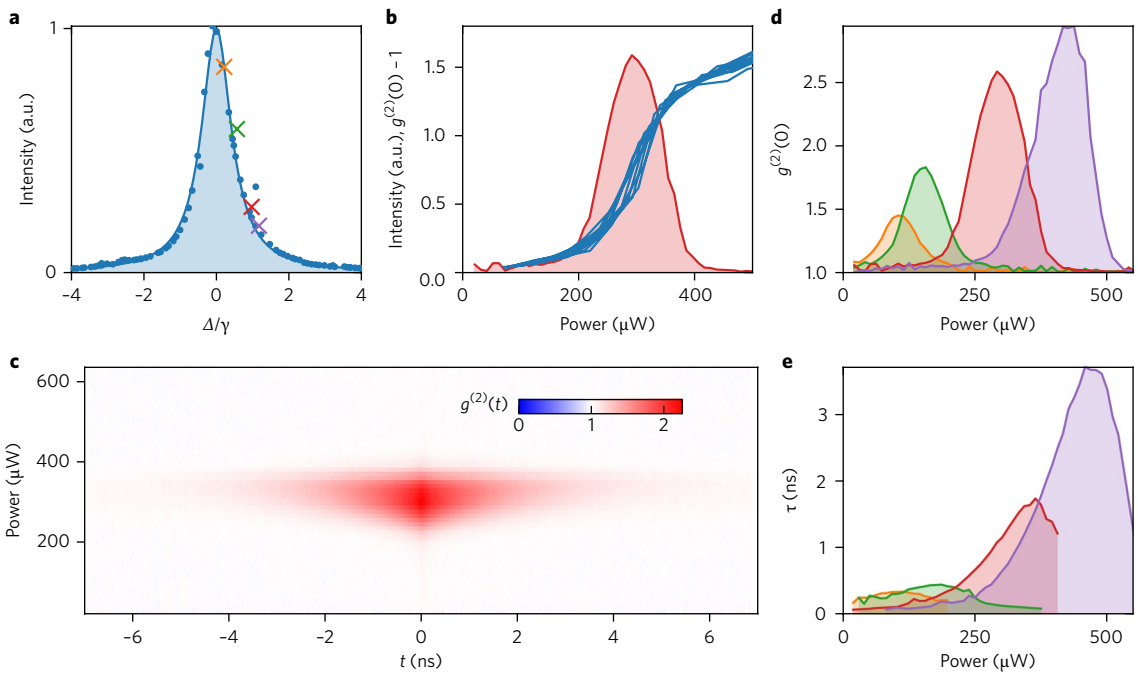

Fig. 3 | Non-equilibrium dynamics in the strong fluctuation regime. a, Normalized polariton transmission spectrum under weak laser drive power of 100 nW as a function of laser detuning. The blue solid line is a Lorentzian fit to the data (blue dots). The crosses indicate the laser detunings, $\Delta/\gamma=0.2$, 0.4, 0.8 and 1.0, where the data in **b**–**e** were taken. **b**, Blue line: transmitted intensity while ramping the excitation power at $\Delta/\gamma=0.8$ (red cross in **a**) up and down repeatedly. Instead of bistability, only a single trace with superlinear behaviour is visible. Red line: bunching amplitude $g^{(2)}(0)-1$ for the same detuning (same data as red line in **d**). Strongest bunching coincides with the onset of superlinear behaviour in a power ramp. **c**, Power-dependent $g^{(2)}(t)$ function for $\Delta/\gamma=0.8$. The slowing down of dynamics is observable through the prolongation of photon bunching at the critical drive strength. **d**,**e**, Bunching amplitude and timescale extracted from power-dependent $g^{(2)}$ measurements for the detunings indicated in **a**.

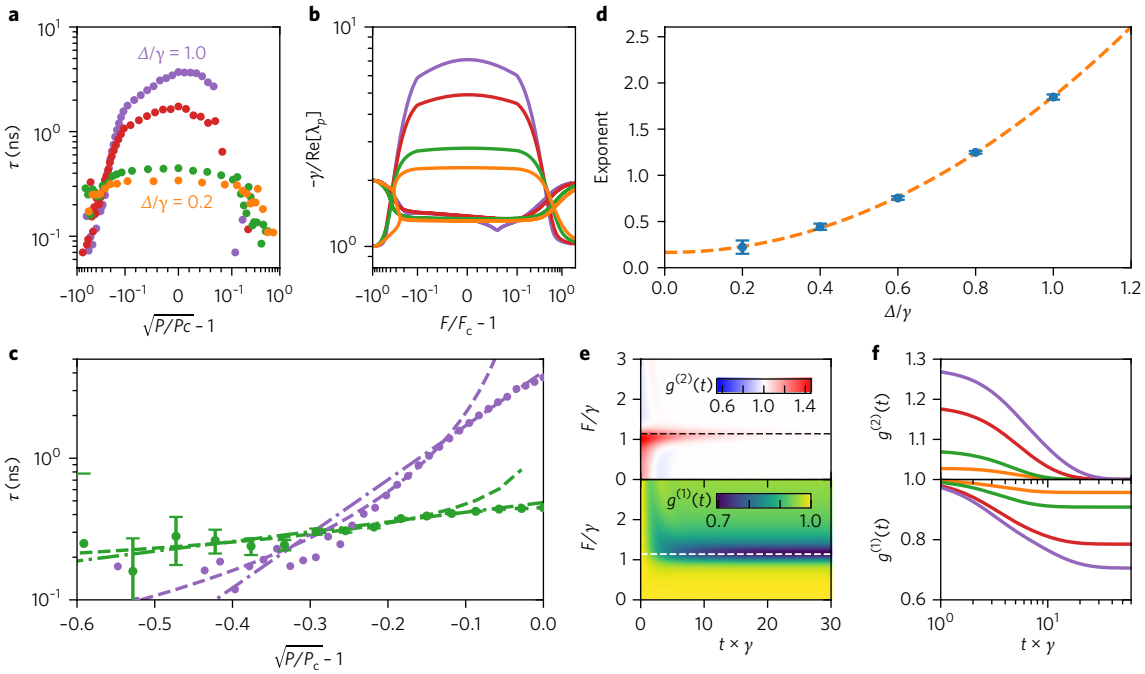

Fig. 4 | Liouvillian gap scaling with drive strength. a, Bunching timescale in the vicinity of the critical drive strength corresponding to the longest observed bunching decay time for each detuning. Different line colours denote detunings $\Delta/\gamma = 0.2$, 0.4, 0.8 and 1.0 (colour code same as in Fig. 3). In the bistable regime, the region where the lines coalesce roughly coincides with the mean-field bistability edge. **b**, Simulation of the lowest three normalized Liouvillian excited state lifetimes for the same detunings and $U/\gamma = 0.2$ showing good qualitative agreement with the data in **a**. **c**, Zoom-in on the region where $\sqrt{P/P_C} - 1 < 0$ in **a**. Dashed lines and dashed-dotted lines denote weighted power-law and exponential fits, respectively. For clarity, only detunings 0.4 (green) and 1.0 (purple) are shown, and error bars (one standard deviation) are displayed only for the green curve. **d**, Exponent of the power-law fits in **c** as a function of laser detuning. Error bars are one standard deviation. The orange dashed line is a weighted quadratic fit. **e**, Simulations of power- and time-dependent $g^{(2)}$ and $g^{(1)}$ functions (top and bottom panels, respectively). Both display qualitative changes when the critical drive strength is reached. The detuning is $\Delta/\gamma = 1.0$ and other parameters are the same as in **b**. **f**, Time-dependent $g^{(2)}$ and $g^{(1)}$ functions (top and bottom panels, respectively) for excitation powers where the longest-lived bunching occurs (line cuts along dashed lines in **e**) for the same detunings as in **a**–**c**.

does not result in a qualitative change in either the bunching amplitude or the decay time (Fig. 3d and e, respectively). The closing of the Liouvillian gap is more pronounced for larger laser detunings where the mean polariton number required to reach the onset of nonlinear response is larger and hence longer-lived bunching occurs (see Supplementary Information). However, the sharp distinction of single and multiple solutions in mean-field theory as a function of laser detuning is washed away by quantum fluctuations that are enhanced by the strong polariton interactions that we estimate to be $U/\gamma \sim 0.03$.

The decay times of the $g^{(2)}(t)$ bunching peak depicted in Fig. 3 are orders of magnitude shorter than those shown in Fig. 2 due to the enhanced nonlinearity and reduced mean polariton number. Naturally, with a slow laser power scan we do not observe bistability even for $\Delta/\gamma = 1.0 > \sqrt{3}/2$. On the other hand, a lack of qualitative differences in bunching and Liouvillian gap closing across the 'mean-field bistability threshold' implies the possibility to observe hysteretic behaviour even for $\Delta/\gamma < \sqrt{3}/2$ if the laser power is ramped up/down faster than the inverse Liouvillian gap[31].

Even though the bunching amplitude and the Liouvillian gap in Fig. 3d,e show a monotonous quantitative change across the bistability threshold for increasing laser detuning, their scaling behaviour as a function of drive strength reveals the signatures of the underlying DPT. Despite the fact that we are dealing with a first-order transition in a zero-dimensional system that is far from the thermodynamic limit, we follow ref. [14] and refer to the drive strength for which the longest-lived bunching is observed as the critical drive $F_C = \sqrt{P_C}$, where and correspond to the drive amplitude and power, respectively, at this point. In a mean-field picture, this drive strength denotes the excitation power for which the transition rate from the lower to the higher occupancy state is equal to the rate of the reverse process, and the bunching time corresponds to the tunnelling time between them[19]. In Fig. 4a, we show the bunching decay timescale as a function of normalized distance to this point. Whereas for second-order phase transitions a dependence $\tau \sim |F/F_C - 1|^{\alpha}$ with a universal exponent α and divergence at the critical point would be expected[32], no such behaviour is known for first-order transitions. Indeed, we find a laser-detuning-dependent finite Liouvillian excited state lifetime $-1/\mathrm{Re}[\lambda_\rho]$ around the critical drive, in good qualitative agreement with numerical simulations (Fig. 4b). In ref. [14], a power-law behaviour was suggested to describe the lifetime scaling when approaching the critical drive. In Fig. 4c, we indeed find good agreement between a power-law fit (dashed lines) and the data in a limited region away from the critical power. We emphasize, however, that using an exponential fit also provides a reasonable description of the whole curve until the critical point (dashed-dotted lines).

For a given polariton–polariton interaction strength, the mean polariton number required to reach the bistable regime increases linearly with Δ/γ, indicating that increasing the laser detuning suppresses the effect of quantum fluctuations. The increase of the power-law exponent with increasing Δ/γ (Fig. 4d) shows that as we in this fashion push the system towards the thermodynamic limit, the Liouvillian gap will close abruptly as the classically bistable region is reached.

The information about the Liouvillian spectrum of driven-dissipative systems could also be obtained using first-order coherence ($g^{(1)}$) measurements. In Fig. 4e, we plot calculated $g^{(2)}$ and $g^{(1)}$ as a function of time and drive strength. Indeed, both exhibit long-lived

deviations from an all-orders coherent response at the critical drive strength and the bunching observed in $g^{(2)}$ corresponds to a decrease of coherence in $g^{(1)}$. Line cuts along the dashed lines, where the longest-lived bunching is observed, are displayed in Fig. 4f and demonstrate that the decay of bunching and coherence are dictated by the same timescale. For the long dynamics observed here, however, a $g^{(1)}$ measurement is experimentally much harder to realize, and may even be infeasible: since interference experiments are sensitive to phase noise, it is highly challenging to introduce sufficiently large delays to probe second-scale dynamics and to ensure phase coherence of the excitation light over such long times. $g^{(2)}$ measurements, on the other hand, are insensitive to phase coherence and are therefore superior from an experimental point of view for problems involving such large dynamic ranges as reported here.

We conclude that measuring $g^{(2)}$ of driven-dissipative systems under near-resonant excitation reveals crucial insights into the underlying non-equilibrium dynamics described by the Liouvillian eigenspectrum. Moreover, this technique is applicable to a whole range of systems from close to thermodynamic limit down to the highly interesting regime where quantum fluctuations are prominent. Applying our $g^{(2)}$-based technique to lattices of interacting photonic systems could pave the way to study the rich field of non-equilibrium quantum many-body dynamics, which recently garnered a lot of interest due to their intriguing steady-state phase diagrams[4,7,33–35].

Methods

Methods, including statements of data availability and any associated accession codes and references, are available at https://doi.org/10.1038/s41567-017-0020-9.

Received: 18 June 2017; Accepted: 8 November 2017;
Published online: 11 December 2017

References

1. Diehl, S. et al. Quantum states and phases in driven open quantum systems with cold atoms. *Nat. Phys.* **4**, 878–883 (2008).
2. Verstraete, F., Wolf, M. M. & Cirac, J. I. Quantum computation and quantum-state engineering driven by dissipation. *Nat. Phys.* **5**, 633–636 (2009).
3. Diehl, S., Tomadin, A., Micheli, A., Fazio, R. & Zoller, P. Dynamical phase transitions and instabilities in open atomic many-body systems. *Phys. Rev. Lett.* **105**, 015702 (2010).
4. Le Boité, A., Orso, G. & Ciuti, C. Steady-state phases and tunneling-induced instabilities in the driven dissipative bose-hubbard model. *Phys. Rev. Lett.* **110**, 233601 (2013).
5. Carmichael, H. J. Breakdown of photon blockade: a dissipative quantum phase transition in zero dimensions. *Phys. Rev. X* **5**, 031028 (2015).
6. Fink, J. M., Dombi, A., Vukics, A., Wallra, A. & Domokos, P. Observation of the photon-blockade breakdown phase transition. *Phys. Rev. X* **7**, 011012 (2017).
7. Wilson, R. M. et al. Collective phases of strongly interacting cavity photons. *Phys. Rev. A* **94**, 033801 (2016).
8. Biondi, M., Blatter, G., Türeci, H. E. & Schmidt, S. Nonequilibrium gas-liquid transition in the driven-dissipative photonic lattice. *Phys. Rev. A* **96**, 043809 (2017).
9. Kessler, E. M. et al. Dissipative phase transition in a central spin system. *Phys. Rev. A* **86**, 012116 (2012).
10. Baas, A., Karr, J. P., Eleuch, H. & Giacobino, E. Optical bistability in semiconductor microcavities. *Phys. Rev. A* **69**, 023809 (2004).
11. Boulier, T. et al. Polariton-generated intensity squeezing in semiconductor micropillars. *Nat. Commun.* **5**, 3260 (2014).
12. Drummond, P. D. & Walls, D. F. Quantum theory of optical bistability. I. Nonlinear polarisability model. *J. Phys. A. Math. Gen.* **13**, 725–741 (1980).
13. Casteels, W., Storme, F., Le Boité, A. & Ciuti, C. Power laws in the dynamic hysteresis of quantum nonlinear photonic resonators. *Phys. Rev. A* **93**, 033824 (2016).
14. Casteels, W., Fazio, R. & Ciuti, C. Critical dynamical properties of a first-order dissipative phase transition. *Phys. Rev. A* **95**, 012128 (2017).
15. Gibbs, H. M., McCall, S. L. & Venkatesan, T. N. C. Differential gain and bistability using a sodium-filled Fabry-Perot interferometer. *Phys. Rev. Lett.* **36**, 1135–1138 (1976).
16. Almeida, V. R. & Lipson, M. Optical bistability on a silicon chip. *Opt. Lett.* **29**, 2387–2389 (2004).
17. Wurtz, G. A., Pollard, R. & Zayats, A. V. Optical bistability in nonlinear surface-plasmon polaritonic crystals. *Phys. Rev. Lett.* **97**, 057402 (2006).
18. Kheruntsyan, K. V. Wigner function for a driven anharmonic oscillator. *J. Opt. B* **1**, 225–233 (1999).
19. Risken, H., Savage, C., Haake, F. & Walls, D. F. Quantum tunneling in dispersive optical bistability. *Phys. Rev. A* **35**, 1729–1739 (1987).
20. Lett, P., Christian, W., Singh, S. & Mandel, L. Macroscopic quantum fluctuations and first-order phase transition in a laser. *Phys. Rev. Lett.* **47**, 1892–1895 (1981).
21. Letscher, F., Thomas, O., Niederprüm, T., Fleischhauer, M. & Ott, H. Bistability versus metastability in driven dissipative Rydberg gases. *Phys. Rev. X* **7**, 021020 (2017).
22. Rodriguez, S. R. K. et al. Probing a dissipative phase transition via dynamical optical hysteresis. *Phys. Rev. Lett.* **118**, 247402 (2017).
23. Kasprzak, J. et al. Bose-Einstein condensation of exciton polaritons. *Nature* **443**, 409–414 (2006).
24. Carusotto, I. & Ciuti, C. Quantum fluids of light. *Rev. Mod. Phys.* **85**, 299–366 (2013).
25. Jacqmin, T. et al. Direct observation of Dirac cones and a flatband in a honeycomb lattice for polaritons. *Phys. Rev. Lett.* **112**, 116402 (2014).
26. Amo, A. et al. Exciton-polariton spin switches. *Nat. Photon.* **4**, 361–366 (2010).
27. Ballarini, D. et al. All-optical polariton transistor. *Nat. Commun.* **4**, 1778 (2013).
28. Hartmann, M. J. Quantum simulation with interacting photons. *J. Optics* **18**, 104005 (2016).
29. Noh, C. & Angelakis, D. G. Quantum simulations and many-body physics with light. *Rep. Prog. Phys.* **80**, 016401 (2017).
30. Carusotto, I. *Linear and Nonlinear Optics in Bose Fields: Light Waves in Dielectric Structures, Matter Waves in Optical Lattices* PhD thesis, Scuola Normale Superiore di Pisa (2000).
31. Goldsztein, G. H., Broner, F. & Strogatz, S. H. Dynamical hysteresis without static hysteresis: scaling laws and asymptotic expansions. *SIAM. J. Appl. Math.* **57**, 1163–1187 (1997).
32. Sachdev, S. *Quantum Phase Transitions*. 2nd edn, (Cambridge Univ. Press, Cambridge, 2011).
33. Jin, J., Rossini, D., Leib, M., Hartmann, M. J. & Fazio, R. Steady-state phase diagram of a driven QED-cavity array with cross-Kerr nonlinearities. *Phys. Rev. A* **90**, 023827 (2014).
34. Mendoza-Arenas, J. J. et al. Beyond mean-field bistability in driven-dissipative lattices: bunching-antibunching transition and quantum simulation. *Phys. Rev. A* **93**, 023821 (2016).
35. Foss-Feig, M. et al. Emergent equilibrium in many-body optical bistability. *Phys. Rev. A* **95**, 043826 (2017).

Acknowledgements

We would like to thank A. Reinhard, T. Volz and J. Reichel for early work that led to the development of the semiconductor fibre cavity structure used in this work. We also acknowledge fruitful discussions with C. Ciuti and S. Zeytinoğlu. This work was supported by the Swiss National Science Foundation (SNSF) through the National Centre of Competence in Research - Quantum Science and Technology (NCCR QSIT). A.S., C.S. and S.H. acknowledge support by the State of Bavaria and the Deutsche Forschungsgemeinschaft within the Project Schn1376/3–1.

Author contributions

T.F. and A.I. designed and supervised the experiment. T.F. carried out the measurements. A.S., S.H., and C.S. grew the sample. T.F. and A.I. wrote the manuscript.

Competing interests

The authors declare no competing financial interests.

Additional information

Supplementary information is available for this paper at https://doi.org/10.1038/s41567-017-0020-9.

Reprints and permissions information is available at www.nature.com/reprints.

Correspondence and requests for materials should be addressed to T.F.

Publisher's note: Springer Nature remains neutral with regard to jurisdictional claims in published maps and institutional affiliations.

Methods

Set-up. The experimental set-up is illustrated in Fig. 1a. The sample consists of an epitaxially grown GaAs λ spacer layer containing a single 17-nm-wide $In_{0.04}Ga_{0.96}As$ QW on top of 34 pairs of AlAs/GaAs distributed Bragg reflectors. It faces a dielectric DBR with 17.5 pairs deposited on the facet of an optical fibre. A Gaussian dimple-shaped surface geometry has been fabricated onto the facet by CO_2 laser ablation prior to coating, such that in addition to the longitudinal confinement of the cavity mode due to the DBRs, also a strong transverse confinement is induced resulting in a zero-dimensional polariton box with discrete eigenstates[36]. Due to a finite ellipticity of the cavity, the photonic mode is split by 180 μeV into two linearly polarized modes out of which only one is addressed by the excitation through careful alignment of the polarization of the incoming light. The transmitted signal is sent to the top of a dewar in a free-space configuration. The sample is mounted in a bath cryostat at 4 K.

Measurements. For excitation, a tunable single-mode diode laser is used. Before being coupled into the set-up, the light passes a noise eater to reduce laser intensity noise. The power values mentioned in the main text correspond to the power sent into the set-up, whereas due to mode mismatch between the plane waves in the fibre core and the intracavity mode, as well as an asymmetric DBR configuration, the incoupling efficiency into the cavity is on the order of 10^{-4}–10^{-3}. The transmitted light is then coupled into an optical fibre and sent to two avalanche photodiodes (APDs) in a HBT configuration to measure both transmission spectra and photon statistics. The time resolution (instrument response function full-width at half-maximum (FWHM)) is 64 ps.

Photon correlations. In Fig. 2, single photon coincidences have been recorded in the so-called time-tagged time-resolved (TTTR) mode of the correlation electronics. This allows us to obtain both time traces and $g^{(2)}$ from the data. To analyse them, we employ different techniques to calculate $g^{(2)}(t)$. For small delays up to 10 ms, we calculate the true single-photon correlation function as defined in equation (4) with a delay bin width of 400 ps. Then, we downsample this data to 10 ns to obtain the curves displayed in Fig. 2d. To restrict the computation time required to treat longer delays, we then bin all photon arrival times into 10 μs windows and calculate the classical intensity autocorrelation function $g^{(2)}_{\mathrm{class}}(t) = \langle I(t')I(t'+t)\rangle \,/\, \langle I(t')\rangle^2$ for longer delays. For the data in Figs. 3 and 4, we directly process and save photon correlation data without recording individual arrival times. To extract the bunching amplitude and timescale we fit an exponentially decaying bunching signature $g^{(2)}(t) = 1 + A\ \exp(-|\,t\,|\,/\tau)$ convolved with the independently measured instrument response function in a time window of ±20 ns to the data. Note that the twofold bunching decay observed in Fig. 2 is not present in the data with increased role of quantum fluctuations in Fig. 3, hence a single decay is sufficient to describe the bunching features and extract the timescales shown in Fig. 4.

Data availability. The data that support the plots within this paper and other findings of this study are available from the corresponding author upon reasonable request.

References

36. Besga, B. et al. Polariton boxes in a tunable fiber cavity. *Phys. Rev. Appl.* **3**, 014008 (2015).